Large Elastic Anisotropy in Brillouin Scattering of Copper-Intercalated GaS and GaSe

Daniel Ramesh Paulo-Wach,[1,2] Ethan Chen,[3] Masaru Nakamura,[4] Oscar D. Dubon,[1,2] and Kristie J. Koski[3,*]

[1] *Department of Materials Science and Engineering, University of California Berkeley California 94720, USA*

[2] *Materials Sciences Division, Lawrence Berkeley National Laboratory, Berkeley, California 94720, USA*

[3] *Department of Chemistry, University of California, Davis, California 95616, USA*

[4] *National Institute for Materials Science (NIMS), 1-1 Namiki, Tsukuba, Ibaraki 305-0044, Japan*

(Dated: December 9, 2025)

Brillouin scattering of bulk layered, hexagonal gallium sulfide (GaS) and gallium selenide (GaSe) were measured both as pristine materials and intercalated with copper and silver. The sound velocities, refractive index, and four of the five independent elastic stiffnesses (c_{ij}) were determined. Values of the c_{11} elastic stiffness in thin crystals are higher than in previous measurements, bringing the elastic anisotropy (c_{11}/c_{33}) into a range typical of other layered materials. Copper intercalation showed a larger effect on acoustic phonons in GaS than GaSe.

The processing of materials can have a significant effect on their physical properties.[1] Gallium sulfide (GaS) and gallium selenide (GaSe) are two-dimensional layered materials with a hexagonal structure that can be grown as either p-type or n-type.[1] Both materials show unique opto-electronic properties with promise in photodetectors, lasers, and elasto-optical applications.[2–4] Additionally, the properties of these materials are highly sensitive to dopants and impurities.[1] GaS and GaSe have been the subject of many previous mechanical, Brillouin and ultrasonic investigations.[5–13] Previously reported Brillouin scattering measurements showed a surprisingly low elastic anisotropy (c_{11}/c_{33}) for a layered material, where the elastic stiffness in the plane was found to only be about three times larger than that in the stacking direction.[6–8, 11] Conversely, most other layered materials have significantly larger reported elastic anisotropy.[14]

Brillouin scattering is a laser-based technique that measures acoustic phonons to extract elastic stiffnesses and sound velocities of materials. The interaction between the incident laser and the sample leads to the Stokes creation or anti-Stokes annihilation of an acoustic phonon with a wavevector $\vec{q}$, visible as a peak in the Brillouin spectra. In a Brillouin scattering experiment, measurements taken at different geometries of incident light, scattered light, and sample angles yield representative spectra peaks of acoustic phonons in different directions. Brillouin scattering data typically shows one strong elastic scattered peak surrounded by Stokes/anti-Stokes pairs of a longitudinal (or quasi-longitudinal) and two transverse (or quasi-transverse) phonon peaks.

We investigate Brillouin scattering of GaS and GaSe and use intercalation of copper to modulate the elastic properties, motivated by the large impact of dopants and impurities on these materials.[1] We also intercalate GaS with silver. While we find values of the out-of-plane c_{33} elastic stiffness are similar to previous measurements, we find significantly different values of the in-plane c_{11} stiffness yielding a larger, but more expected, elastic anisotropy than previous measurements.[6–8, 11] We show that intercalation of silver and copper has a significant impact on the acoustic phonons of GaS but not much impact in GaSe.

Bulk GaS crystals were grown via the Bridgman method following Nakamura et al.[15], and bulk GaSe crystals are legacy crystals from Cradley Crystals Corporation. All samples were exfoliated to thinner dimensions ($\lesssim 0.3$ mm) using a razor blade to separate the layers. Crystals were intercalated with copper and silver using similar processes detailed in Koski et al.[16, 17] Samples were suspended in free space for measurement. Brillouin scattering was collected with a scanning, tandem, multi-pass Sandercock TFP-1 with a Coherent Verdi V6 $NdYVO_4$ laser at $\lambda_o = 532$ nm with a 20X SLWD Mitutoyo objective (N.A. = 0.42) for collection with laser powers of ~ 7 mW on the sample for GaS and ~ 3 mW on the sample for GaSe. In 90° geometries, a 10x Mitotoyo was used for focusing. Finesse was approximately 100-300. Acquisition times were on the order of 5-10 minutes for GaS (1100 counts) and several hours for GaSe. Regions of higher intercalant concentration were measured by looking for higher signal intensity, which is theorized to originate from some form of plasmonic enhancement.[18, 19] XRD was collected on a Bruker Eco Advance with a Cu Kα source. Intercalant concentration was determined using X-ray photoelectron spectroscopy (XPS) with a Kratos Axis Supra with an Al anode and scanning electron microscope energy dispersive x-ray spectra (SEM-EDX) on a FEI Scios Dual Beam FIB/SEM with an Oxford X-MaxN EDX detector. Raman spectra were collected from a home-built Raman system with a Princeton Instruments SCT320, 1800 groove/mm grating, and Pixis CCD, with a 532 nm Coherent Sapphire SF laser at 15 mW.

Figure 1 shows characterization of Cu-intercalated GaS and GaSe and Ag-intercalated GaS. GaS and GaSe both have hexagonal crystal structures.[1] XRD (Fig 1a,b) was acquired on the flakes used for Brillouin scattering. The thin single-crystal GaS and GaSe flakes show the (00l)

* koski@ucdavis.edu

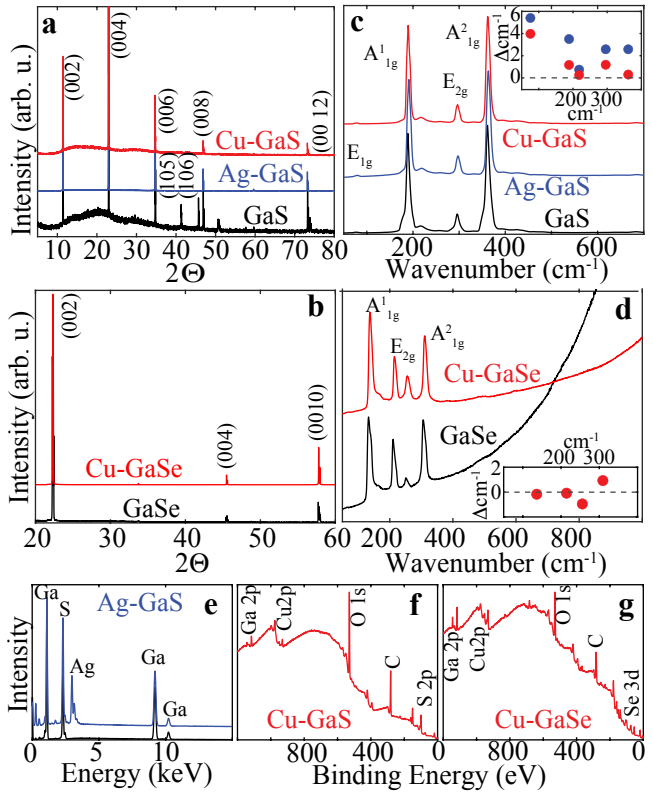

FIG. 1. (a) XRD of GaS pristine and intercalated with Ag and Cu, (b) XRD of GaSe and intercalated with Cu, (c) Raman scattering of GaS and intercalated with Ag and Cu Inset: Shift of Cu- and Ag-GaS raman peaks relative to GaS. Uncertainties are within the data point. (d) Raman scattering of GaSe pristine and intercalated with Cu. Cu intercalation suppresses the GaSe photoluminescence edge. Inset: Shift of Cu-GaSe Raman peaks relative to GaSe. Uncertainties are within the data point. (e) SEM-EDX of Ag-intercalated GaS, (f) XPS wide spectra of Cu-GaS and (g) Cu-GaSe.

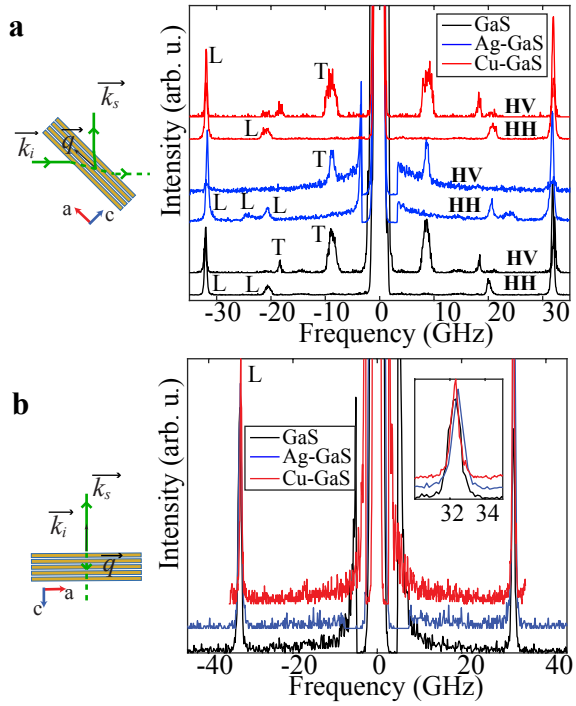

FIG. 2. Brillouin scattering of GaS pristine and intercalated with Ag (blue) and Cu (red) in a (a) 90a geometry using HH and HV polarizers to identify longitudinal and transverse acoustic modes and (b) 180 geometry. Inset shows the stiffening of the longitudinal acoustic phonon with intercalation. $\vec{k_i}$ is incident light; $\vec{k_s}$ is scattered light; and $\vec{q}$ is the probed wavevector

peaks, limiting structural determination to the c lattice constant which is in the direction of the layer stacking. The c-axis of GaS ($c = 15.49 \pm 0.01$ Å) shows negligible change with intercalation of Cu-GaS ($c = 15.50 \pm 0.01$ Å) and Ag-GaS ($c = 15.50 \pm 0.01$ Å). GaSe ($c = 15.96 \pm 0.01$ Å) also shows negligible change upon intercalation of Cu-GaSe ($c = 15.95 \pm 0.01$ Å). Intercalation generally leads to an initial contraction in the host followed by an expansion[20]. Using SEM-EDX, the intercalant concentrations were silver at 0.1 atm % in GaS, Cu at 0.6 atm % in GaS, and Cu at 0.2 atm % in GaSe.

As noted by previous studies, wavenumber shifts in Raman scattering spectra of intercalated materials are often complex, demonstrating either optical phonon stiffening or softening as a result of expansion or contraction of the host, local polarizability changes from the intercalant, and the guest/host donor/acceptor nature.[19, 21, 22] Figure 1c,d show the Raman spectra of intercalated GaS and GaSe, respectively. An inset is provided showing the change in wavenumber shift from the unintercalated host. In GaS (Fig 1c), Cu and Ag intercalation in GaS leads to an increase in the Raman shifts while intercalation of Cu in GaSe increases some Raman shifts and decreases others. The Raman spectra of GaSe (Fig 1d) show a large broad peak at higher wavelengths due to the strong photoluminescence in GaSe.[23] Intercalation of Cu in GaSe quenches or shifts the photoluminescence as seen with the decrease of the strong edge of this peak.

As hexagonal crystals, both GaSe and GaS have an elastic stiffness tensor with five independent stiffnesses (c_{ij}) given by Eq. 1,

$$c_{ij} = \begin{bmatrix} c_{11} & c_{12} & c_{13} & 0 & 0 & 0 \\ c_{12} & c_{11} & c_{13} & 0 & 0 & 0 \\ c_{13} & c_{13} & c_{33} & 0 & 0 & 0 \\ 0 & 0 & 0 & c_{44} & 0 & 0 \\ 0 & 0 & 0 & 0 & c_{44} & 0 \\ 0 & 0 & 0 & 0 & 0 & c_{66} \end{bmatrix} \quad (1)$$

where $c_{12} = c_{11} - 2c_{66}$.[24] Several scattering geometries, and various tilts or rotations from those scattering geometries, were used to extract as many elastic stiffness tensor elements as possible. Diagrams of the primary scattering geometries [25] can be found in Figure 2 and Figure 3. In a 90a geometry (Fig 2a), the input light and scattered light are placed at ∼90 degrees to each other.

The sample is rotated between the input and scattered light such that the $\vec{q}$ is in the ab-plane of the crystals probing in that direction yielding the c_{11} stiffness value. In a backscattering geometry (Fig 2b), the input and scattered light are oriented normal to the surface of the sample. This orientation of input and scattered light on the sample measures Brillouin scattering in the stacking direction and gives the c_{33} stiffness value. In a 90r geometry, the crystal is placed such that the $\vec{q}$ probes down the c-axis correcting for index of refraction differences in the sample (Fig 3b) with respect to the incoming beam and scattered light such that $\vec{q}$ is along the c-axis. This probes the same direction as backscattering but allows appearance of transverse modes, which are eliminated by symmetry in backscattering. Mode assignment was made using cross (HV gives T) and parallel (HH gives L) polarizers in a 90a scattering geometry (Fig 2a). L identifies longitudinal or quasi-longitudinal modes and T identifies transverse or quasi-transverse modes. Two longitudinal acoustic modes were found in GaS at ~ 31 GHz and ~ 22 GHz. The mode at 31 GHz also shows up in the Brillouin backscattering measurement (Fig 2b) and can be assigned as a spontaneous backscattering mode,[26] leaving the 22 GHz mode identified as a genuine 90a longitudinal mode. This type of spontaneous Brillouin backscattering has been known to occur in thin samples.[26] Two transverse modes are identified in GaS under HV polarization. In Ag-intercalated GaS, a third longitudinal mode is observed, possibly due to intermediate structures and incomplete staging similar to that suggested in 20 which could also be caused by localized islanding of the intercalant in the sample with regions of localized expansion; intercalant levels are low enough for large separation in island regions. The second transverse mode in 90a in Ag-GaS vanishes; however, we are able to extract the sound velocity as that transverse mode also appears in 90r scattering. Brillouin backscattering (Fig 2b, inset) shows only minor ($\sim \pm 0.4$ GHz) acoustic phonon stiffening in the stacking direction with intercalation. The acoustic phonons in the 90a scattering direction correspond to c_{11} (longitudinal), c_{44} (transverse), and c_{66} (transverse) and can be used to find c_{12}. Thus, these two primary scattering geometries (90a, 180) are complementary and allow measurement of the acoustic phonons down the a (Fig 2a) and c axes (Fig 2b) and determination of all the elastic stiffnesses except c_{13}. Acquisition of Brillouin scattering in GaSe required significant time (hours to days) due to very low signal (Fig 3). Just as in GaS, three primary scattering geometries were used (90a, 180, and 90r).

The sound velocity, V, can be calculated from the Brillouin frequency shift, $\Delta\nu$, the refractive index, n, the laser wavelength λ_o, and the scattering angle Θ as measured inside the material (Eq 2).

$$V = \frac{|\Delta\nu|\lambda_o}{2n\sin\left(\frac{\Theta}{2}\right)} \tag{2}$$

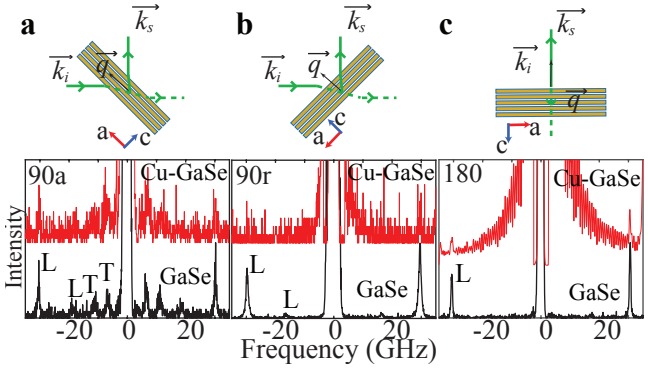

FIG. 3. Brillouin scattering of pristine (black) and Cu-intercalated (red) GaSe in a (a) 90a (b) 90r, and (c) 180 scattering geometry.

For geometries used in this study, this formula evaluates to:

$$V_{90a} = \frac{|\Delta\nu|\lambda_o}{\sqrt{2}};\ V_{180} = \frac{|\Delta\nu|\lambda_o}{2n};\ V_{90r} = \frac{|\Delta\nu|\lambda_o}{\sqrt{4n^2-2}} \tag{3}$$

The stiffness tensor element is calculated from the sound velocity, given a density ρ by Eq 4. A density of 3860 kg/m^3 is used for GaS and 5030 kg/m^3 for GaSe.[7, 9, 27] Liquid gradient density techniques can be used to find the density of a material,[19] however GaS and GaSe have densities of 3860-5040 kg/m^3 which is far above what that method can measure. As concentrations of intercalant are low, we assume small to no density change.

$$c_{ij} = V^2\rho \tag{4}$$

The longitudinal sound velocity V is the same for 180 and 90r measurements, as both measure in the stacking direction (c), and allows determination of the refractive index n, but this technique is prone to large error We found that GaS $n = 2.5 \pm 0.1$; AgGaS $n = 2.6 \pm 0.1$; CuGaS $n = 2.5 \pm 0.1$; GaSe $n = 2.5 \pm 0.1$; CuGaSe $n = 2.5 \pm 0.1$. The wavelength dependent refractive index of GaS has been carefully measured by Yael et al.[28] which, interpolated, yields a refractive index of 2.65 at 532 nm, which was used for sound velocity calculations here, and 2.6 for GaSe from Wasscher et al.[5] Wide variability is found in reported values of refractive index.[5, 10, 28] The 90r geometry is also used to extract c_{44} in Ag-GaS where the corresponding transverse mode appeared in the 90r measurement but not the 90a.

The crystal is rotated in a 90a geometry (Fig 4a) to ensure that the $\vec{q}$ is measured in the plane. Since the crystals are hexagonal, there should be no deviation in frequency shift throughout a 180 degree rotation. Figures 4a through 4c show the frequency shifts of the acoustic phonons in pristine and intercalated GaS; a line is

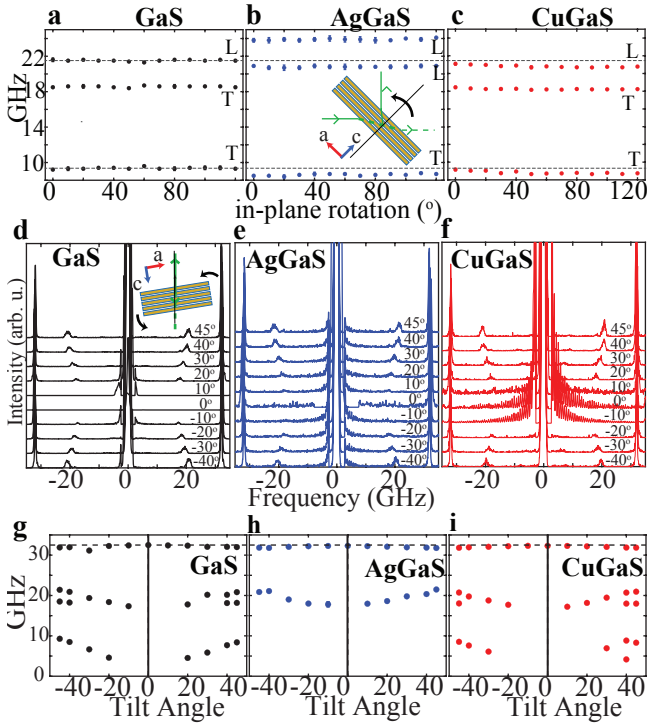

FIG. 4. Brillouin frequency shifts of (a) GaS, (b) Ag- and (c) Cu-intercalated GaS rotated in a 90a geometry to verify that acoustic phonons measured are all in the *ab*-plane with modes showing almost no variation. Backscattering spectra as a function of sample tilt of (d) GaS, (e) Ag-intercalated GaS, (f) Cu-intercalated GaS and (g) Brillouin frequency shifts of GaS, (h) Ag-intercalated GaS, and (i) Cu-GaS.

drawn for the frequency shifts of pristine GaS. Intercalation of silver results in two longitudinal modes with one greater frequency than GaS and one at lower frequency. Intercalation of Cu notably decreases the Brillouin frequency shifts of all acoustic phonon modes in the plane.

Table I presents the sound velocities from Brillouin scattering: the longitudinal velocity in the ab-plane (V_{La}, giving c_{11}) and along the stacking direction (V_{Lc}, giving c_{33}), as well as the pure-transverse velocities for shear in the ab-plane (V_{Ta_1}, giving c_{66}), and in the ac-plane (V_{Ta_2}, giving c_{44}). Values of the sound speed match well with recent measurements which found $V_{Lc} = 3140 \pm 20 m/s$ in GaS.[12] Intercalation of metals into GaS and GaSe does not affect the sound velocity in the stacking direction as found in Brillouin scattering investigations of other intercalated layered materials.[19, 21, 22, 29]

GaS was tilted in the backscattering geometry to break symmetry and access the transverse acoustic phonon in the *ac*-plane which would give V_{Ta_2} yielding c_{44} in the extrapolated limit of small tilt angles. Fig 4 shows the tilt of the sample in 180 backscattering along with peak positions for GaS (Fig 4a,b), AgGaS (Fig 4c,d), and CuGaS (Fig 4 e,f). In principle, the variation with tilt angle (-50° to 50°; $\sin^{-1}(\sin 50°/n) \approx 18°$) provides information about c_{13}, but due to the fairly large refractive index, the thinness of the crystal, and the uncertainties in the other stiffness tensor elements, it was not possible to extract a meaningful c_{13} value. Cu-GaSe (Fig 4f) shows noise peaks from excess laser light entering the TFP-1 at and near normal incidence.

TABLE I. Sound velocity of GaS, GaSe and metal intercalated GaS and GaSe in m/s (error in parenthesis).

	V_{La}	V_{Lc}	V_{Ta_1}	V_{Ta_2}
GaS	8069(31)	3284(26)	3517(46)	1877(10)
Ag-GaS	8992(76); 7837(72)	3186(158)	3244(39)	1740(12)
Cu-GaS	6867(23)	3280(7)	3319(21)	1499(12)
GaSe	7058(48)	3223(1)	4180(38)	2496(102)
Cu-GaSe	6901(376)	3214(10)	4357(56)	2569(10)

TABLE II. Elastic stiffnesses, c_{ij} in GaS and GaSe in GPa from compared to Polian et al.[8] and Chiang et al.[6]

	c_{11}	c_{33}	c_{44}	c_{66}	c_{12}	c_{11}/c_{33}
GaS	251(2)	41.6(7)	13.6(1)	47.7(1)	156(4)	6.0
Ag-GaS	312(5)	39(4)	11.7(2)	41(1)	231(7)	8.0
Cu-GaS	182(1)	41.5(2)	8.7(1)	42.5(5)	96.9(2)	4.4
GaS [8]	122	38	9.8	44.3	33.4	3.2
GaSe	251(3)	37.8(1)	12.2(1)	31(3)	188(9)	6.6
Cu-GaSe	240(26)	37.6(2)	11.8(0.2)	33(1)	173(27)	6.4
GaSe [6]	105	35.1	10.4	36.3	32.5	3.0

Table II gives the elastic stiffnesses, c_{ij}, for pristine and intercalated GaS and GaSe. Values of the out-of-plane longitudinal elastic stiffness (c_{33}) match well with recent measurements which found $c_{33} = 38.1 \pm 0.5$ GPa.[12] Effects of intercalation on the acoustic phonons of layered crystals are complicated.[22] Similar to almost all other measurements of Brillouin scattering of intercalated layered materials, the intercalation affects the in-plane stiffness more than the plane-normal stiffness.[19, 21, 22, 29]

We find significantly larger in-plane sound velocity and elastic stiffness (c_{11}) yielding larger elastic anisotropy (c_{11}/c_{33}) than previous measurements, displayed in Table II. Values for c_{11} derived from previous measurements[8] predict a longitudinal mode at 15 GHz in Figure 2; instead, we find a longitudinal mode much higher at ∼20 GHz. There are several explanations possible: (i) sample growth differences coupled with impurities, (ii) overlapping longitudinal modes from successive orders in older techniques, (iii) issues with scattering geometries that do not measure in the correct direction, or (iv) failure to properly identify mode assignments such as with using polarizers. Previous measurements had disagreement in elastic stiffness values using different techniques.[8, 13] It is possible that the first published measurements may have biased later results.[9, 10, 13, 27, 30]

Previous experiments by Polian et al.[8] used "up to 5 passes with the Tropel Inc Model FP-100 Fabry-Perot

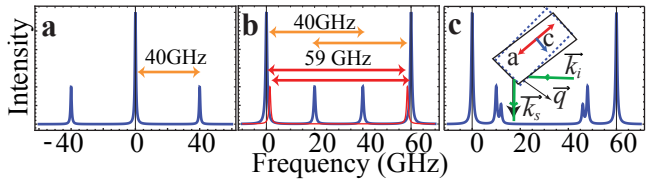

FIG. 5. (a) Schematic illustration of collection using a Sandercock TFP. (b) Mode misassignment possible with older interferometry techniques. Modes can be misaligned in frequency shift because of overlapping frequency ranges (yellow) including being hidden by the elastic peak (red). (c) Geometry used by Chiang et al.[6]

interferometer." This is a multi-pass transmission instrument that yields inelastic peaks between two successive elastic mode; it is possible to mistakenly reference a Brillouin peak to the wrong elastic mode, or have overlap of an inelastic mode within the elastic peak giving an incorrect frequency shift. The advances from the Sandercock design of the tandem multi-pass Fabry-Perot interferometer (TFP-1 and TFP-2) eliminate overlapping order modes so only a single elastic peak is seen with minor, nearly invisible doublet ghost peaks from adjacent orders. Honma et al.[9] used a similar system and published the raw data that make it possible to observe the overlapping order issue and possible peak misassignment.[9] Figure 5a shows an example of the kind of spectra that would be seen in the TFP-1 Sandercock design which makes it easy to identify the single strong elastic peak and the inelastic peaks referenced to it. Figure 5b shows an example of the kind of spectra that might be observed using a Tropel Model FP-100, with two elastic peaks appearing at 0 and 60 GHz, each of which serves as a zero reference for its own set of inelastic peaks. Such spectra could easily be misinterpreted by referencing each inelastic peak to the wrong elastic peak (yielding an incorrect measurement of 20 GHz in this example, when the correct Brillouin shift should be 40 GHz). Honma et al.[9] observed other peaks at high frequency that went unassigned, which could belong to a mode with a sound velocity of 8069 m/s, as we measure.[9] Also, it is possible that a limited free spectral range used in previous studies would result in a longitudinal mode overlapping the elastic mode, obscuring observation of a mode with a large sound speed in the *ab*-plane.[9] Overlap of orders and misassignments of longitudinal and transverse peaks is something that has long contaminated Brillouin results and is especially prevalent in systems that use single or double non-scanning etalons or VIPAs.[25]

Another issue could be measuring down an incorrect axis. Figure 5 shows a representative schematic that is similar to the drawing of Chiang et al. used in measuring GaSe in a 90a geometry.[6] In this geometry, the input beam is at an angle to the *c*-axis of the crystal and the scattered light is out the *a*-normal face of the crystal. The $\vec{q}$-vector ends up being between *a* and *c*, thus giving a much lower sound velocity in that direction. In this study, we rotated the crystal in a 90a geometry to ensure the $\vec{q}$-vector is in the plane and often found we sometimes had to redo measurements many times. Previous studies did not have a technique at the time to ensure that the $\vec{q}$-vector was measuring only in the plane. Finally, previous measurements may not have used a polarizer to identify mode assignments, leading to misassigned modes.

There are other issues that could account for the differences in measured anisotropy, such as differences in growth technique, sample handling, dopants, or contamination. The significant effect that impurities and sample quality have on sound velocity and stiffness in GaS was noted by Gatulle et al.[13] in ultrasonic measurements, with reported sound velocities ranging almost ± 1000 m/s across different samples. In contrast, we found a similar longitudinal sound velocity across different samples, but there was clearly some minor sample-to-sample variation. No major impurities were detected with EDX in GaS or GaSe. GaS grown via iodine vapor transport as in Polian et al.[7, 8] can have an impurity concentration of up to 10 ppm, significantly affecting properties as revealed by Brillouin scattering.[1, 8] Bridgman-grown GaS crystals in this work show broader Raman modes in pristine versus intercalated, suggesting impurities or defects, which are removed by chemical treatment in the intercalation process, narrow observed Raman modes. Intercalation at very small amounts radically affects the elastic stiffness of GaS, demonstrating that even the smallest of impurities has a strong effect on elastic properties in this material.

In terms of previous crystal preparation,[6–8] the crystal was measured at a polished edge to access phonon wavevectors located in the *ab*-plane of GaS needles. We attempted to polish the edges to access these additional angles as well. We found that polishing the edges frayed the crystal at the layer edge, such that the acoustic modes we detected were still often in the *c*-direction or some combination, thereof, not accessing pure *ab*-plane modes.

In conclusion, this study finds a large elastic anisotropy (c_{11}/c_{33}) in GaS and GaSe crystals, which differs from previously reported values for GaS and GaSe but is consistent with the strong anisotropy observed in other two-dimensional layered materials. Intercalation has a significant, but complicated, effect on the sound velocity and elasticity in these materials, similar to the large effect on other properties of GaS and GaSe.[1]

DATA AVAILABILITY

Data available on request from the authors.

ACKNOWLEDGMENTS

The authors acknowledge funding from the National Science Foundation NSF-DMR-2202472 and NSF-DMR-2500503. DPW acknowledges funding support from the

National GEM Consortium. MN acknowledges GaS growth support by JSPS KAKENHI Grant Number 24K08274. The authors thank B. W. Reed for useful conversations.

[1] R. M. A. Lieth, *Preparation and crystal growth of materials with layered structures*, Vol. 1 (Springer Science & Business Media, 1977).

[2] T. Barker, A. Gray, M. Weir, J. Sharp, A. Kenton, Z. Kudrynskyi, H. Rostami, and A. Patané, npj Flexible Electronics **9**, 2 (2025).

[3] Y. Sun, Z. Ren, Z. Zhao, F. Zhang, and F. Xing, ACS Applied Nano Materials **8**, 8712 (2025).

[4] S. Ahmed, P. K. Cheng, J. Qiao, W. Gao, A. M. Saleque, M. N. Al Subri Ivan, T. Wang, T. I. Alam, S. U. Hani, Z. L. Guo, *et al.*, ACS nano **16**, 12390 (2022).

[5] J. Wasscher and J. Dieleman, Physics Letters A **39**, 279 (1972).

[6] T. Chiang, J. Dumas, and Y. Shen, Solid State Communications **28**, 173 (1978).

[7] A. Polian, J. M. Besson, M. Grimsditch, and H. Vogt, Applied Physics Letters **38**, 334 (1981).

[8] A. Polian, J. Besson, M. Grimsditch, and H. Vogt, Physical Review B **25**, 2767 (1982).

[9] Y. Honma, M. Yamada, K. Yamamoto, and K. Abe, Journal of the Physical Society of Japan **52**, 2777 (1983).

[10] N. C. Fernelius, *Properties and bibliography of GaSe*, Tech. Rep. (1994).

[11] M. Fischer, A. Polian, A. Chevy, and J. Chervin, Solid state communications **56**, 311 (1985).

[12] W. Al-Basheer, C. Viernes, R. Zheng, S. Netzke, K. Pichugin, and G. Sciaini, ACS omega **9**, 47475 (2024).

[13] M. Gatulle, M. Fischer, and A. Chevy, physica status solidi (b) **119**, 327 (1983).

[14] M. Ren, J. Z. Liu, L. Wang, and Q. Zheng, arXiv preprint arXiv:1405.4086 (2014).

[15] M. Nakamura, H. Nakamura, K. Shimamura, and N. Ohashi, Journal of Crystal Growth **573**, 126303 (2021).

[16] K. J. Koski, J. J. Cha, B. W. Reed, C. D. Wessells, D. Kong, and Y. Cui, Journal of the American Chemical Society **134**, 7584 (2012).

[17] K. J. Koski, C. D. Wessells, B. W. Reed, J. J. Cha, D. Kong, and Y. Cui, Journal of the American Chemical Society **134**, 13773 (2012).

[18] W. Robertson, A. Moretti, and R. Bray, Physical Review B **35**, 8919 (1987).

[19] B. W. Reed, C. Tran, and K. J. Koski, Physical Review Materials **7**, 044003 (2023).

[20] A. Powell, Annual Reports Section" C"(Physical Chemistry) **90**, 177 (1993).

[21] B. W. Reed, V. Huynh, C. Tran, and K. J. Koski, Physical Review B **102**, 054109 (2020).

[22] B. W. Reed, E. Chen, and K. J. Koski, Nano Letters **24**, 11954 (2024).

[23] S. Quan, Y. Wang, Y. Liang, J. Jiang, B. Zhong, K. Yu, H. Zhang, and G. Kan, The Journal of Physical Chemistry C **124**, 10185 (2020).

[24] J. F. Nye, *Physical properties of crystals: their representation by tensors and matrices* (Oxford university press, 1985).

[25] P. Bouvet, C. Bevilacqua, Y. Ambekar, G. Antonacci, J. Au, S. Caponi, S. Chagnon-Lessard, J. Czarske, T. Dehoux, D. Fioretto, *et al.*, Nature Photonics **19**, 681 (2025).

[26] Y. Takagi and R. W. Gammon, Journal of applied physics **61**, 2030 (1987).

[27] B. Powell, S. Jandl, J. Brebner, and F. Levy, Journal of Physics C: Solid State Physics **10**, 3039 (1977).

[28] Y. Gutierrez, D. Juan, S. Dicorato, G. Santos, M. Duwe, P. H. Thisen, M. Giangregorio, F. Palumbo, K. HIngerl, C. Cober, *et al.*, Dieletric function crystalline 2H-GaS (2022).

[29] B. W. Reed, D. R. Williams, B. P. Moser, and K. J. Koski, Nano letters **19**, 4406 (2019).

[30] G. Belen'kiĭ, E. Y. Salaev, and R. Suleĭmanov, Soviet Physics Uspekhi **31**, 434 (1988).